VII International Conference on Computational Methods in Marine Engineering
MARINE 2017
M. Visonneau, P. Queutey and D. Le Touzé (Eds)

A NEW ADJUSTMENT-FREE DAMPING METHOD FOR FREE-SURFACE WAVES IN NUMERICAL SIMULATIONS

JANEK MEYER*, KAI GRAF† AND THOMAS SLAWIG§

*Yacht Research Unit Kiel
R&D-Centre Univ. Applied Sciences Kiel
Schwentinestrasse 24, 24149 Kiel, Germany
e-mail: Janek.Meyer@yru-kiel.de, web page: http://www.yru-kiel.de

† University of Applied Sciences Kiel
Department of Mechanical Engineering
Grenzstrasse 3, 24149 Kiel, Germany
e-mail: kai.graf@fh-kiel.de - Web page: http://www.fh-kiel.de

§ Kiel University
Algorithmic Optimal Control
Christian-Albrechts-Platz 4, 24118 Kiel, Germany
e-mail: ts@informatik.uni-kiel.de - Web page: http://www.algopt.informatik.uni-kiel.de

Key words: Damping of free-surface waves, Volume-of-Fluid method, RANSE, OpenFOAM

Abstract. Simulating free-surface flow around ships in sea waves using RANSE-Methods usually requires damping of the waves in front of the outlet to avoid reflections. It has been shown, that common damping methods like sponge layer methods deliver a reliable damping for monochromatic waves, but require a parameter adjustment by the user for different wave scales. The paper describes a new wave damping method which delivers results of same accuracy (reflections less than 2%) but does not require a manual user adjustment. The method is based on damping the vertical velocity component to reduce wave propagation. This is done by implicitly relaxing this component to zero. The relaxation is implemented with the deferred correction approach. The method is implemented in our own in-house OpenFOAM solver, which is a RANSE code using the volume of fluid method and a SIMPLE-like algorithm for the solution. Verification is done in 2D for waves of different scales, steepness, computational meshes and damping zone measures. A comparison to a linear sponge layer approach is given for the different wave scales. The 2D simulations show, that the best wave damping is achieved with the same relaxation function parameters for each individual wave. A 3D application to a modern yacht in head waves is presented. All simulation results show that the new method delivers a reliable wave damping without any parameter adjustment. The method is particularly applicable for flows with waves of different scales, like sea waves superposed with the wave system generated by a yacht.

1 INTRODUCTION

Predicting the motion of and the flow around yachts in waves using RANSE-solvers is not very common for flow analysis of sailing yachts. One of the obstacles is the generation of proper waves using free-surface flow methods. Especially the outlet of the flow domain produces unwanted reflections of the waves without using proper methods. Different methods suppressing such reflections have been developed leading from satisfying to unsatisfying results.

One group of damping methods can be classified as sponge layer methods. They are based on a damping-zone next to the boundary in which a source term is added to the governing equations. The source term usually weakens the vertical component of the fluid velocity which prevents the wave of moving through this zone. This methods deliver a good result with reflections less than 2% but require a parameter adjustment by the user.

Another way using a damping zone is presented in [1]. It explicitly relaxes the velocity to zero and the volume fraction to values of an undisturbed free-surface. This method introduces some numerical problems due to the explicit manipulation of the results of the Reynolds-averaged Navier-Stokes equations.

In [2] a method suppressing reflections at the outlet based of active filtering is presented. This method manipulates the outlet boundary condition without using a damping-zone. Indeed the damping quality is not satisfying and reflection up to 15% occure.

A lot of approaches preventing wave reflections have been given, but to the authors knowledge none of them deliver a reliable quality without parameter adjustment.

Wave damping is not only interesting for ships in waves. Also the simulation of free-surface flow around ships without sea waves may benefit of a wave-damping method. Here, the waves generated by the ship are reflected and inhibits a 100% steady-state solution. Stretching the grid in front of the outlet will prevent reflections, but a proper wave-damping method might reduce the effort for the user. Furthermore simulating offshore structures in waves require an adequate method to prevent wave reflections.

2 GOVERNING EQUATIONS AND SOLUTION METHOD FOR FREE-SURFACE FLOW

For the calculation of the free-surface flow the incompressible unsteady Reynolds-averaged Navier-Stokes equations are solved using the finite volume method. The Volume-of-Fluid (VOF) method introduced in [3] is used for the calculation of the free-surface. The momentum conservation equation (employ the eddy-viscosity hypothesis for closure), the mass conversation and the conservation equation for the transport of the volume fraction α are defined as

$$\frac{\partial \rho \mathbf{u}}{\partial t} + \nabla \cdot (\rho \mathbf{u}\mathbf{u}) - \nabla \cdot \mu_e \left(\nabla \mathbf{u} + (\nabla \mathbf{u})^T \right) = -\nabla p + \rho \mathbf{g} \tag{1}$$

$$\nabla \cdot \mathbf{u} = 0 \tag{2}$$

$$\frac{\partial \alpha_i}{\partial t} + \nabla \cdot (\alpha_i \mathbf{u}) = 0 \tag{3}$$

with the volume fraction α_i for the ith fluid of the two phases water and air, the velocity vector $\mathbf{u}$, the pressure p, the gravity vector $\mathbf{g}$, the density ρ and the effective dynamic viscosity μ_e. The flow properties are then calculated by $\rho = \sum_i \rho_i \alpha_i$, $\mu = \sum_i \mu_i \alpha_i$ and $1 = \sum_i \alpha_i$. The free-surface

is defined by the volume fraction $\alpha = 0.5$. The linearized, semi-discretized momentum equation can be written as

$$a_\mathrm{d}\mathbf{u}_\mathrm{d}^{q+1} + \sum_n a_\mathrm{n}\mathbf{u}_\mathrm{n}^{q+1} = -\nabla p^q + \mathbf{s}_{\mathrm{w/o\ p}} \quad . \tag{4}$$

Here, a represents the elements of the coefficient matrix $\mathbf{A}$ and the subscripts d and n mark the main diagonal- and neighbor-elements. All sources and contributions to the right hand side except the pressure gradient are included in $\mathbf{s}_{\mathrm{w/o\ p}}$. The solution of the current SIMPLE-iteration is marked with $q+1$ and the solution of the last iteration with q. We will not distinguish between the first prediction of the velocity and the corrected velocity of the same iteration. Rearranging (4) to $\mathbf{u}_c$ yields the velocity equation:

$$\mathbf{u}_\mathrm{d}^{q+1} = \frac{1}{a_\mathrm{d}} \left(-\nabla p^{q+1} + \mathbf{s}_{\mathrm{w/o\ p}} - \sum_n a_\mathrm{n}\mathbf{u}_\mathrm{n}^q \right) \quad . \tag{5}$$

Substituting and rearranging (5) into (2) yields the poisson equation for the pressure:

$$\nabla \cdot \left(\frac{1}{a_\mathrm{d}} \nabla p^{q+1} \right) = \nabla \cdot \frac{1}{a_\mathrm{d}} \left(\mathbf{s}_{\mathrm{w/o\ p}} - \sum_n a_\mathrm{n}\mathbf{u}_\mathrm{n}^q \right) \quad . \tag{6}$$

After integrating over the volume, the Gauss Theorem is used to transform the volume-integrals to surface-integrals. Face-variables are then interpolated with second-order discretization schemes. The pressure and its gradient is reconstructed with a method for arbitrary unstructured grids given in [4]. This prevents smearing of the density induced jump behavior at the free-surface. This includes the jump in the characteristic of the surface normal gradient of the pressure at the free-surface. Discretization in time is done with OpenFOAM's backward scheme, which is a full-implicit, second-order scheme based on quadratic interpolation using the values of two old time steps. The convective-term of the volume-of-fluid equation is discretized with the *Blended Interface Capturing Scheme with Reconstruction* (BRICS) as described in [5]. The rigid body motion is calculated with an in house motion-solver for OpenFOAM considering virtual added mass as described in [6]. This guarantees solver stability and a optimal convergence behavior even for relatively light ships like sailing-yachts. The motion-solver has been implemented and shared with us by FluidEngineeringSolutions GmbH & Co. KG, Germany. The equations are solved in a segregated algorithm and following steps are done in each time step; (A) if required solve motion eqs., (B) solve VOF-equation, (C) solve momentum predictor, (D) solve pressure eq., (E) update flux and velocity, (F) solve turbulence equations. Inside step (D) the pressure eq. may be solved a number of times for non-orthogonal correction. Steps (D) to (E) may be repeated to apply a Piso-like Correction. Steps (A) to (F) are repeated and yield the typical outer iterations of the SIMPLE-algorithm. The momentum and VOF equations are relaxed implicitly. The new solution of the pressure is relaxed explicitly before correcting the velocity. A detailed description of the solver and solution method is given in [7].

3 COMMON WAVE DAMPING METHODS

Two widely used reliable wave damping methods have been described in [8] and [9], whereby the first will be described here. The method is based on a sponge layer which can be derived

by the typical equations for porous media. The damping is achieved by adding a source term to the momentum equation inside a user-defined damping-zone in front of the outlet. The source term is added to the vertical z-component of the momentum equation and can be written as

$$s_{\mathrm{z}}^{\mathrm{d}} = -\rho \left(f_1 + f_2 |u_{\mathrm{z}}| \right) w u_{\mathrm{z}} \tag{7}$$

with the weight-function

$$w = \frac{e^{\kappa} - 1}{e^{1} - 1} \tag{8}$$

and the character of the blending function

$$\kappa = \left(\frac{x - x_{\mathrm{sd}}}{x_{\mathrm{ed}} - x_{\mathrm{sd}}} \right)^{\zeta} \tag{9}$$

with ζ usually set to 3.5. Here ρ is the density of the fluid and u_z is the the vertical velocity component. The parameter f_1 gives the amount of linear damping, f_2 the amount of quadratic damping. The weight factor w depends on the location inside the domain and helps to smoothly fade in the source term in the damping zone. The wave propagation direction is given by x with x_{sd} as the start and x_{ed} as the end x-coordinate of the damping zone.
This method is implemented in commercial codes like STAR-CCM+ or in a slightly different form in ANSYS Fluent. It has been deeply investigated in [10] and it has been shown, that the method delivers a reliable damping with satisfying damping quality. Nevertheless the parameters f_1 and f_2 have to be adjusted for different waves. Scaling laws for adjusting these parameters are also given in [10]. Assuming optimal chosen parameters for a regular and monochromatic wave adjustment is necessary if the wave changes in its scale. Where no adjustment is required if the computational mesh or wave steepness is changed. Also no adjustment is required for different lengths of the damping zone. However, the maximal achievable damping quality depends on this length and at least two wavelengths are recommended.

4 DERIVATION OF THE NEW WAVE DAMPING METHOD

In [1] wave damping is achieved by relaxing the velocity $\mathbf{u}$ and the volume fraction α explicitly after solving for the volume fraction. Explicit relaxation is done with the generic equation

$$\phi_{\mathrm{relaxed}} = r\phi + (1 - r)\phi^{\mathrm{t}} \ . \tag{10}$$

Here ϕ is an generic quantity, the superscript t signifies the target value. The relaxation factor r depends on above mentioned damping weight w:

$$r = 1 - w \ . \tag{11}$$

The method delivers a good damping quality but has significant disadvantages. All three velocity components are relaxed to zero. The volume fraction is relaxed to values which assume an undisturbed flat free-surface at constant height. This forbids additional current or boat speed superposing with the orbital velocity of the waves. Additionally this delivers some kind of Dirichlet boundary condition (BC) at the outlets, whereby a Neumann BC is desirable. Furthermore

such an explicit relaxation will prevent the convergence of the SIMPLE-algorithm. Still, this relaxation approach and the sponge layer approach described in section 3 are the inspiration for our method. Our goal is to reduce the vertical velocity component by the use of an implicit relaxation included in the momentum equation. Considering the discretized momentum equation $\mathbf{A} \cdot \mathbf{u} = \mathbf{s}$ with the coefficient matrix $\mathbf{A}$, the velocity vector $\mathbf{u}$ and all explicitly treated terms on the right hand side included in the source $\mathbf{s}$, implicit relaxation of all velocity components can be done with

$$\frac{1}{r} a_\mathrm{d} \mathbf{u}_\mathrm{d}^{q+1} + \sum_n a_\mathrm{n} \mathbf{u}_\mathrm{n}^{q+1} = \mathbf{s} + \frac{1-r}{r} a_\mathrm{d} \mathbf{u}_\mathrm{d}^\mathrm{t} \ . \tag{12}$$

Here, the subscripts d marks the main diagonal- and n the neighbor-elements of $\mathbf{A}$. As the limiting case, where the relaxation factor r tends to zero the convergence of the equation system is not obvious. Adopting L'Hôpital's rule twice one can show that $\mathbf{u}_\mathrm{d}^{q+1}$ tends to $\mathbf{u}_\mathrm{d}^\mathrm{t}$ as aspired. Modifying equation (12) to relax only the vertical velocity component is not straightforward. Using this approach the coefficient matrix $\mathbf{A}$ has to be modified. Indeed it is common practice to reuse this matrix for all three components. Therefore manipulating $\mathbf{A}$ only for the vertical component will produce additional calculation effort and a lot of programing effort to implement this methods into existing numerical codes like OpenFOAM. To solve this problem our idea is to implement the implicit relaxation with the help of the deferred correction approach. That means, the product of the modified matrix and the velocity is treated explicitly on the right hand side. Additionally the product of the unmodified matrix and the velocity is added on both, explicit and implicit, sides leading to the original unmodified left hand side. If the equation system is converging, the terms with the unmodified matrix are canceling each other out and the solution depends only on the modified matrix. This allows to modify only the right hand side, more precisely only the z-component of the right hand side. In the following we will describe two approaches to use the deferred correction. The first approach might be the obvious way to go but leads to a diverging equation system, as it will be shown. The second approach leads to our final damping method and a converging equation system.

4.1 First Approach (divergent)

In the following equations all terms on the left hand side consider the unknown velocity from the current iteration $q+1$ and all terms on the right hand side use the known values of the last iteration q. For convergence the velocity u^q should tend to $u^{\mathrm{q}+1}$. Starting from the z-component of the vector equation (12)

$$\frac{1}{r} a_\mathrm{d} u_\mathrm{zd}^{q+1} + \sum_n a_\mathrm{n} u_\mathrm{zn}^{q+1} = s_\mathrm{z} + \frac{1-r}{r} a_\mathrm{d} u_\mathrm{zd}^\mathrm{t} \tag{13}$$

and applying $a_\mathrm{d} u_\mathrm{zd}$ on both sides leads to

$$\frac{1}{r} a_\mathrm{d} u_\mathrm{zd}^{q+1} + a_\mathrm{d} u_\mathrm{zd}^{q+1} + \sum_n a_\mathrm{n} u_\mathrm{zn}^{q+1} = s_\mathrm{z} + \frac{1-r}{r} a_\mathrm{d} u_\mathrm{zd}^\mathrm{t} + a_\mathrm{d} u_\mathrm{zd}^q \ . \tag{14}$$

Putting the term $\frac{1}{r} a_\mathrm{d} u_\mathrm{zd}^{q+1}$ from the left to the right hand side changes its iteration index and leads to

$$a_\mathrm{d} u_\mathrm{zd}^{q+1} + \sum_n a_\mathrm{n} u_\mathrm{zn}^{q+1} = s_\mathrm{z} + \frac{1-r}{r} a_\mathrm{d} u_\mathrm{zd}^\mathrm{t} + a_\mathrm{d} u_\mathrm{zd}^q - \frac{1}{r} a_\mathrm{d} u_\mathrm{zd}^q \ . \tag{15}$$

Simplifying this equation delivers the final equation for the first approach

$$a_\mathrm{d} u_\mathrm{zd}^{q+1} + \sum_n a_\mathrm{n} u_\mathrm{zn}^{q+1} = s_\mathrm{z} + \frac{1-r}{r}\left(a_\mathrm{d} u_\mathrm{zd}^\mathrm{t} - a_\mathrm{d} u_\mathrm{zd}^q\right) \quad . \tag{16}$$

The whole relaxation of the z-component for the velocity is included in one source term on the right hand side. Therefore it is no more necessary to manipulate the coefficient matrix **A** and it is possible to include the relaxation of the z-component in the typical vector form of the momentum equation used in codes like OpenFOAM.

4.2 Investigation on the convergence behavior - 1st approach

Using the Jacobi method to solve equation (16) leads to

$$u_\mathrm{zd}^{q+1} = \frac{1}{a_\mathrm{d}}\left(s_\mathrm{z} + \frac{1-r}{r}\left(a_\mathrm{d} u_\mathrm{zd}^\mathrm{t} - a_\mathrm{d} u_\mathrm{zd}^q\right) - \sum_n a_\mathrm{n} u_\mathrm{zn}^q\right) \quad . \tag{17}$$

For wave damping ($u_\mathrm{zd}^\mathrm{t} = 0$) with full relaxation ($r \to 0$) the source term s_z becomes negletable and the solution of the equation is $u_\mathrm{zd}^{q+1} \to -\infty u_\mathrm{zd}^q$. Therefore no convergence is possible for small r.

4.3 Second Approach

For the second approach equation (13) is multiplied with the relaxation factor r before applying the deferred correction

$$a_\mathrm{d} u_\mathrm{zd}^{q+1} + r\sum_n a_\mathrm{n} u_\mathrm{zn}^{q+1} = r s_\mathrm{z} + (1-r)\, a_\mathrm{d} u_\mathrm{zd}^\mathrm{t} \quad . \tag{18}$$

In eq. (13) of the first approach the main diagonal elements of **A** are multiplied with $\frac{1}{r}$. Now, in eq. (18) the neighbor elements of **A** and the right hand side term s_z are multiplied with r. Applying the deferred correction method to eq. (18) to get rid of the relaxation factor on the left hand side leads to

$$a_\mathrm{d} u_\mathrm{zd}^{q+1} + \sum_n a_\mathrm{n} u_\mathrm{zn}^{q+1} = r s_\mathrm{z} + (1-r)\left(a_\mathrm{d} u_\mathrm{zd}^\mathrm{t} + \sum_n a_\mathrm{n} u_\mathrm{zn}^q\right) \quad . \tag{19}$$

Here, the original right hand side term s_z is manipulated. This needs to be considered in the derivation of the pressure equation. Our solution how to consider this as easy as possible is described in subsection 4.5.

4.4 Investigation on the convergence behavior - 2nd approach

Using the Jacobi method again to solve eq. (19) gives

$$u_\mathrm{zd}^{q+1} = \frac{1}{a_\mathrm{d}}\left(r s_\mathrm{z} + (1-r)\left(a_\mathrm{d} u_\mathrm{zd}^\mathrm{t} + \sum_n a_\mathrm{n} u_\mathrm{zn}^q\right) - \sum_n a_\mathrm{n} u_\mathrm{zn}^q\right) \quad . \tag{20}$$

For full relaxation ($r \to 0$) one gets the aspired behavior $u_\mathrm{zd}^q \to u_\mathrm{zd}^\mathrm{t}$ where u_zd^t is zero for wave damping.

4.5 Manipulation of the original right hand side

Using equation (19) requires to manipulate the original right hand side s_z including the terms depending on the pressure p. Therefore it is necessary to build a new pressure equation. This can be done straightforward but is not our finally chosen way. For the sake of completeness this way will be given here, first. Afterward a simpler way leading to our final method will be described.

First way:
The vector form of the momentum equation considering the wave damping method can be written as:

$$a_\mathrm{d}\mathbf{u}_\mathrm{d}^{q+1} + \sum_n a_\mathrm{n}\mathbf{u}_\mathrm{n}^{q+1} = \mathbf{R}\cdot\left(-\nabla p^q + \mathbf{s}_{\mathrm{w/o\ p}}\right) + \mathbf{s}^* \quad . \tag{21}$$

Here, $\mathbf{s}_{\mathrm{w/o\ p}}$ is the original right hand side without the pressure gradient ($\mathbf{s} = -\nabla p + \mathbf{s}_{\mathrm{w/o\ p}}$). The tensor $\mathbf{R}$ allows to manipulate only the z-component of the equation and is defined as $\mathbf{R} = \begin{bmatrix} r_\mathrm{x} & 0 & 0 \\ 0 & r_\mathrm{y} & 0 \\ 0 & 0 & r_\mathrm{z} \end{bmatrix}$ with the relaxation factors $r_\mathrm{x} = r_\mathrm{y} = 1.0$ and $r_\mathrm{z} = r$ for the three Cartesian directions. The source term $\mathbf{s}^*$ is defined as

$$\mathbf{s}^* = (\delta_{ij} - \mathbf{R})\cdot\left(a_\mathrm{d}\mathbf{u}_\mathrm{d}^\mathrm{t} + \sum_n a_\mathrm{n}\mathbf{u}_\mathrm{n}^q\right) \tag{22}$$

with the Kronecker-delta $\delta_{ij} = \begin{bmatrix} 1 & 0 & 0 \\ 0 & 1 & 0 \\ 0 & 0 & 1 \end{bmatrix}$. Rearranging eq. (21) for $\mathbf{u}_\mathrm{d}^{q+1}$ leads to the new velocity equation allowing to calculate the corrected velocity $\mathbf{u}_\mathrm{d}^{q+1}$

$$\mathbf{u}_\mathrm{d}^{q+1} = \frac{1}{a_\mathrm{d}}\left(\mathbf{R}\cdot\left(-\nabla p^{q+1} + \mathbf{s}_{\mathrm{w/o\ p}}\right) + \mathbf{s}^* - \sum_n a_\mathrm{n}\mathbf{u}_\mathrm{n}^q\right) \quad . \tag{23}$$

Substituting the velocity of the continuity equation (2) with (23) and rearranging gives the adopted pressure equation

$$\nabla\cdot\left(\frac{1}{a_\mathrm{d}}\mathbf{R}\cdot\nabla p^{q+1}\right) = \nabla\cdot\frac{1}{a_\mathrm{d}}\left(\mathbf{R}\cdot\mathbf{s}_{\mathrm{w/o\ p}} + \mathbf{s}^* - \sum_n a_\mathrm{n}\mathbf{u}_\mathrm{n}^q\right) \quad . \tag{24}$$

Second way:
For the second way the momentum equation is written in a way containing the unmodified right hand side $\mathbf{s}$ and an additional source term

$$a_\mathrm{d}\mathbf{u}_\mathrm{d}^{q+1} + \sum_n a_\mathrm{n}\mathbf{u}_\mathrm{n}^{q+1} = \underbrace{-\nabla p^q + \mathbf{s}_{\mathrm{w/o\ p}}}_{\mathbf{s}} + \mathbf{s}_\mathrm{wavedamping} \tag{25}$$

with

$$\mathbf{s}_\mathrm{wavedamping} = (\delta_{ij} - \mathbf{R})\cdot\left(\nabla\tilde{p}^q - \mathbf{s}_{\mathrm{w/o\ p}} + a_\mathrm{d}\mathbf{u}_\mathrm{d}^\mathrm{t} + \sum_n a_\mathrm{n}\mathbf{u}_\mathrm{n}^q\right) \quad . \tag{26}$$

It is important to notice, that the pressure gradient is used in two terms. To build the pressure equation it is only solved for the pressure of the original right hand side $\mathbf{s}$. The pressure gradient inside the source term for the wave damping $\mathbf{s}_{\text{wavedamping}}$ is fixed and therefore marked with a tilde. The equation for the corrected velocity becomes

$$\mathbf{u}_{\text{d}}^{q+1} = \frac{1}{a_{\text{d}}} \left(-\nabla p^{q+1} + \mathbf{s}_{\text{w/o p}} + \mathbf{s}_{\text{wavedamping}} - \sum_n a_{\text{n}} \mathbf{u}_{\text{n}}^{q} \right) \tag{27}$$

and the pressure equation becomes

$$\nabla \cdot \left(\frac{1}{a_{\text{d}}} \nabla p^{q+1} \right) = \nabla \cdot \frac{1}{a_{\text{d}}} \left(\mathbf{s}_{\text{w/o p}} + \mathbf{s}_{\text{wavedamping}} - \sum_n a_{\text{n}} \mathbf{u}_{\text{n}}^{q} \right) \quad . \tag{28}$$

Because $\mathbf{s}_{\text{wavedamping}}$ contains the pressure of the last iteration p^q the solution of the pressure could be interpreted as deferred inside the wave damping zone.

This is our final wave damping method made up of only one additional source term. The original right hand side $\mathbf{s}$ can be pre-calculated and then reused to build the wave-damping source term $\mathbf{s}_{\text{wavedamping}}$. The weight function w included in the relaxation factor r has not the final form and will be substituted with the optimized function w_{opt} as described in chapter 6.3.

5 WAVE GENERATION

At the inlet the values for the velocities and volume fractions are prescribed according to the wave theory. An equation for the pressure value itself or the pressure gradient is missing, which is a significant problem. Our solution is using a Neumann boundary condition with a zero gradient for the pressure. Certainly, the assumption of a zero gradient is wrong in the presence of a wave and for many 3D simulations the wave will collapse behind the inlet. Therefore we are using an relaxation zone behind the inlet and apply full implicit relaxation for the momentum and volume-of-fluid equation. The relaxation factor has the reversed characteristic of the relaxation factor of the damping-zone. Therefore full relaxation is applied at the inlet going to no relaxation at the end of the generation-zone. The target values $\mathbf{u}^{\text{t}}$ and α^{t} are calculate with the chosen wave theory for example 5th-order Stokes. All three velocity components are relaxed to the target value by using equation (12). The relaxation for the volume fraction is applied in the same way

$$\frac{1}{r} a_{\text{VOF d}} \alpha_{\text{d}}^{q+1} + \sum_n a_{\text{VOF n}} \alpha_{\text{n}}^{q+1} = s_{\text{VOF}} + \frac{1-r}{r} a_{\text{VOF d}} \alpha_{\text{d}}^{\text{t}} \tag{29}$$

with the diagonal elements $a_{\text{VOF d}}$ and neighbor elements $a_{\text{VOF n}}$ of the coefficient matrix of the volume-of-fluid transport equation. The term s_{VOF} contains all possible source terms or contributions to the right hand side.

We have not systematically tested different zone length, but a length of 1.0λ produces a reliable wave generation for all of our simulations.

The free-surface is initialized wave-less in the hole domain. For the wave generation we are using the T-soft-parameter of the waves2Foam library. This generates a wave growing from a smooth surface to the full height over the given time T_{soft} in the generation-zone. The growing time T_{soft} is set to the wave-period T. Due to the relaxation approach, the relaxation factor

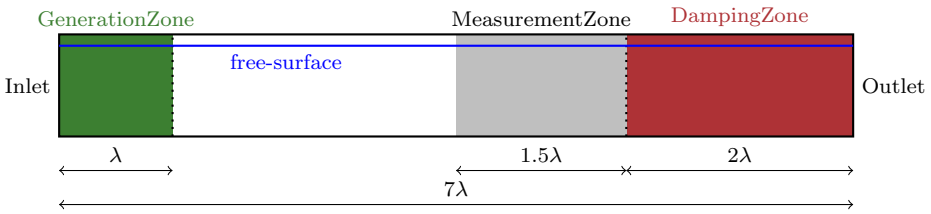

Figure 1: 2d Simulation Setup - clinched in z-direction

becomes small at the end of the generation zone. Therefore, while growing the wave gets smeared at the end of the zone, because the values are set to the new height only partially which leads to very small oscillations in the wave. Still this is acceptable and our best method to produce waves. The oscillations are quantified in chapter 6.

6 VERIFICATION AND WEIGHT FUNCTION OPTIMIZATION

To estimate the damping quality of our method a test-case very close to the one presented in [10] has been chosen. The test-case is also used to optimize the function for the relaxation factor for monochromatic waves. Additionally we have implement the typical sponge layer method for comparison.

6.1 Numerical Simulation Setup

The test-case is based on a 2D wave tank. Figure 1 shows the domain and its measurements. The wave is generated in the generation zone with a length of 1λ. Afterward the wave is propagated through a region of length 4.0λ. Finally the wave damping is applied in the damping zone of length 2.0λ. The Reflections are measured inside the measurement zone in front of the damping zone as explained later. The domain has a height of 4.5λ filled with water up to 4.0λ. The grid has a resolution of 20 cells per wave-height and 100 cells per wave-length as recommended in [10] which refers to [11]. The grid is coarsened with growing distance to the wave. The waves are generated by prescribing volume fractions and velocities of 5th-order Stokes waves at the inlet boundary and in the generation zone as explained in chapter 5. A Neumann boundary condition (BC) with zero gradient is applied for the pressure at the inlet. A free slip wall is applied at the bottom. Indeed, instead of using the hydrostatic pressure gradient a Dirichlet BC with given hydrostatic pressure is applied for the pressure at the bottom. This is done to prevent problems with the preservation of the position of the free-surface. Same BC is applied at the top with the exception, that the velocity BC is set to a zero gradient BC to get a behavior as an open water tank. At the outlet a zero gradient BC is applied for all variables. This allows a lowered free-surface at the outlet or a wave traveling through the outlet.

The solver is using a time step of about $\frac{1}{500}$ of the wave period and 10 SIMPLE-Loops. The pressure is relaxed by 0.3, the velocity by 0.7 and the volume fraction by 0.9. The simulation is assumed to be laminar and no turbulence-model is applied.

Simulations have been done for different wave scales; a medium sized wave with $\lambda = 4.0$m and $H = 0.16$m, a small wave with $\lambda = 0.04$m and $H = 0.0016$m and a big wave with $\lambda = 400$m and $H = 16.0$m. To compare the dependency of the wave steepness a steep wave with $\lambda = 0.4$ and $H = 0.16$ has been simulated. The grid has been scaled accordingly.

The influence of the grid is investigated by using a coarse grid with 10 cells per wave height and 50 cells per wave length for the medium sized wave. The influence of the damping zone length is investigated by also using a damping zone with a length of 1λ for the medium sized wave. The grid is the same as for the initial, medium sized wave simulation. The measurement zone is also kept at the initial position.

6.2 Quantifying the damping quality

To quantify the damping quality, the maximal and minimal wave heights $H_{\max}$ and $H_{\min}$ are measured in the measurement zone in the time interval $[22.0T, 24.0T]$ at 40 evenly distributed times. These wave heights are used to build a reflection coefficient as suggested in [12]

$$C_{\mathrm{R}} = \frac{H_{\max} - H_{\min}}{H_{\max} + H_{\min}} \ . \tag{30}$$

For perfect wave reflection of 100% the coefficient C_{R} becomes 1.0 and zero for no reflection. Considering that the wave train moves with the half speed of a single wave, the chosen time interval allows, that the wave train propagates from the inlet to the outlet and after reflection back to the measurement zone. The wave height is estimated by measuring the minimal and maximal z-Position of the free surface inside the measurement zone. Please notice, that the reflection coefficient includes the wave reflections, but also wave oscillations originating from the wave generation. Additionally a wave, flattening inside the measurement zone due to an insufficient discretization of time or of the convective term will influence the reflection coefficient. The superposition of all these phenomenons may influence the coefficient negatively, but also positively. Reflections may occur at the outlet but also inside or at the beginning of the damping zone, due to too much dampening. To estimate the background oscillations (BO) originating from the wave generation and the influence of flattening all simulations have been done without wave damping but with a long domain of length 25.0λ.

6.3 Optimizing the weight function

The weight function given in equation (8) does not necessarily guarantee the least reflections. Looking at equation (7) of the sponge layer method one can interpret the parameters f_1 and f_2 as a scaling of the weight function w for the different waves. To allow an optimization for our method we are also scaling the weight function with the new introduced scale factor χ

$$w_{\mathrm{opt}} = \chi w \ . \tag{31}$$

The scale factor χ is varied from 0.008 to 1.0 for each wave to achieve the least reflections and to show the dependency of our wave damping method from the wave characteristics.

6.4 Results

Figure 2 shows the results of all simulations. Sub-figure b shows the results of the common linear sponge layer method (with $f_2 = 0.0 = const$), also implemented in our solver. The results are remarkable close to the results presented in [10] using the same method but implemented in StarCCM+. The black, dashed line shows the limit of $C_{\mathrm{R\,lim}} = 0.02$ for an acceptable

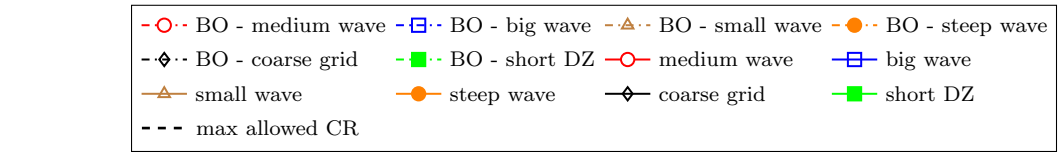

(a) Legend

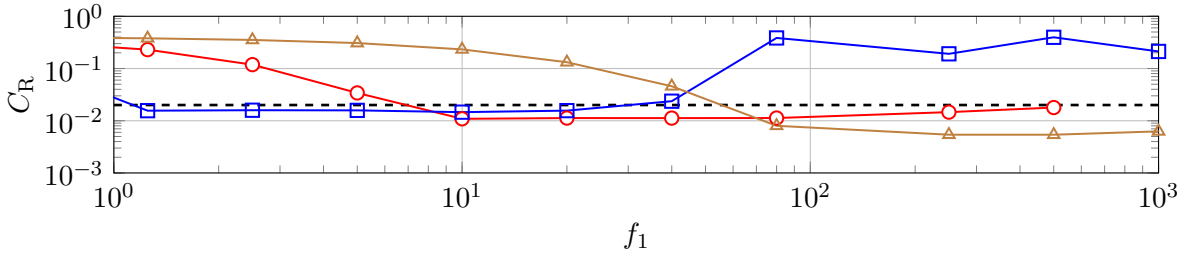

(b) Sponge Layer Method for different wave scales

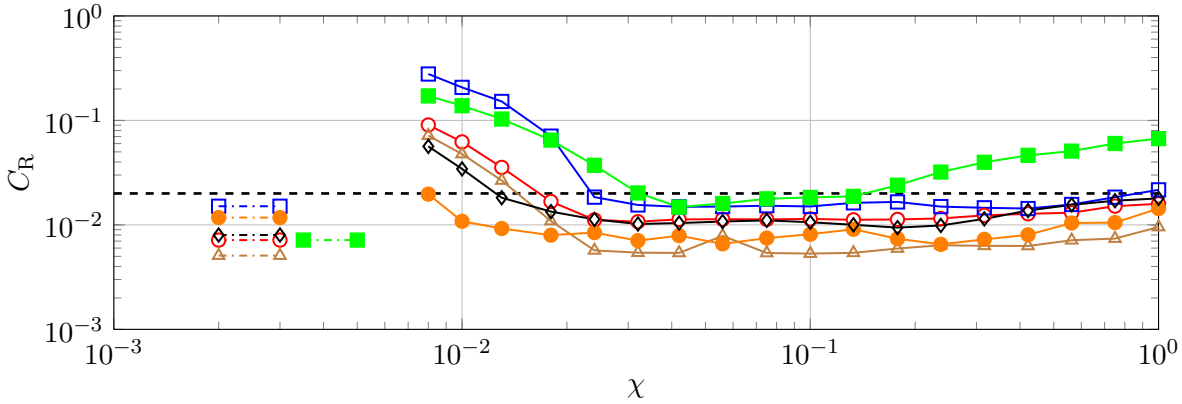

(c) New method log scale

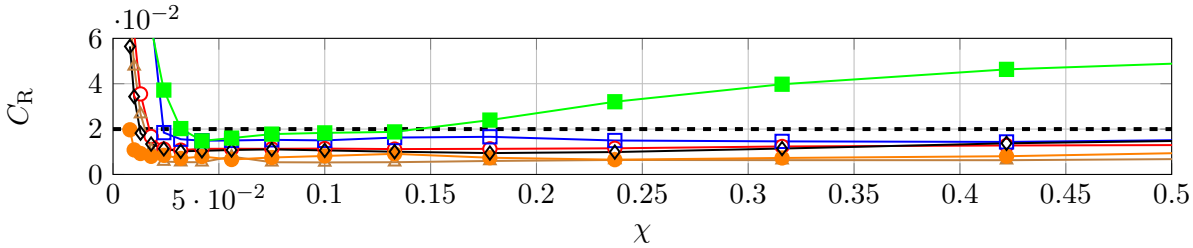

(d) New method linear scale

Figure 2: Reflection coefficient for different wave damping method and different waves

small wave: $\lambda = 0.04$m, $H = 0.0016$m; medium wave: $\lambda = 4.0$m, $H = 0.16$m; big wave: $\lambda = 400$m, $H = 16.0$m; steep wave: $\lambda = 0.4$m, $H = 0.16$m

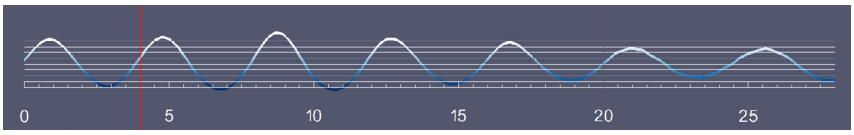

Figure 3: 2D-Wave at $t = 40s$, no damping

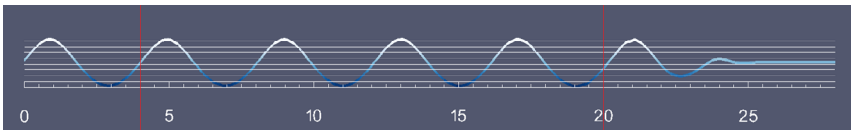

Figure 4: 2D-Wave at $t = 40s$, damping with $\chi = 1.0$ (too much damping)

reflection. Here, the sponge layer method has only been used for different wave scales and one can clearly see that f_1 has to be adjusted to achieve an acceptable reflection. For the quadratic sponge layer method we would like to refer to the results of [10], showing that f_2 has to be adjusted, too. Sub-figure c shows the results of our new method with both axis scaled logarithmically. The initial background oscillations (BO) are marked with a dashed line in the left area of the diagram. All background oscillations are below the maximal allowed value. This shows that the oscillations produced by the wave generation method mentioned in chapter 5 are acceptable. All curves show the same characteristics and an optimal wave damping is achieved for approximately $0.03 \leq \chi \leq 0.15$. The absolute minimum of each curve corresponds with the background oscillations. Only the simulation with the short damping zone clearly shows a worse damping quality. Additionally the absolute minimum for the steep wave deceeds the corresponding background oscillations. A clear reason can not be given but it is possible that the background oscillations and the reflections are canceling each other out.

The characteristics of the curves can be interpreted in that way, that the increasing reflections in the area $\chi < 0.03$ are reflections which arises predominantly at the outlet due to too little damping and that the increasing reflections in the area $\chi > 0.15$ are reflections which arises predominantly at the beginning or inside the wave damping zone due to too fast wave damping.

Sub-figure d shows the same results as c but with a linear scale. This should emphasize graphically that all curves have the same characteristics. Therefore our wave damping method allows to use the same weight function for all different monochromatic waves and no user adjustment is required. To make short damping zones practical we recommend a scale factor χ of about 0.09. Nevertheless we recommend a damping zone with a length of $2.0\lambda_{\max}$ where $\lambda_{\max}$ should be the largest wave length of a given wave spectrum. One can assume that the evaluation of the damping quality would turn out much better without the presence of the background oscillations.

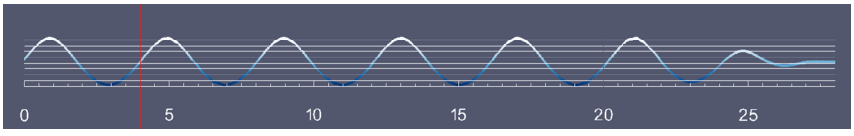

Figure 5: 2D-Wave at $t = 40s$, damping with $\chi = 0.1$ (optimal damping)

Figures 3 to 5 show the wave shapes for different damping parameters. The end of the generation-zone (left) and the beginning of the damping-zone (right) are marked with vertical red lines. Figure 3 shows the wave after $40s$ without any wave-damping applied, leading to reflections of 42%. One can clearly see the reflections superposing with the original wave. Figure 4 shows the result arising due to too much damping, which still leads to only 1.6% reflection. Here, the free-surface becomes completely flat in front of the outlet. Figure 5 shows the wave shape arising due to optimal wave-damping leading to only 1.1% reflection. Here, still a very small wave reaches the outlet. Compared to 4, this will even more reduce reflections at the beginning of the damping-zone. Furthermore, possible reflections from the outlet will be damped while traveling back through the damping-zone.

7 APPLICATION TO A YACHT IN HEAD WAVES

This section shows an application of the new wave damping method to a yacht in head waves. This is a good example for the superposition of the sea waves with the small waves of the yacht and furthermore with the velocity of the yacht.

The yacht is a Class 40 (C40) designed by VPLP, France, and has a length over surface of LoS = 12m. The waves have a length of $\lambda = 18$m, a height of $H = 0.4$m and a period of $T = 3.489$s. Second order Stokes theory is used for wave generation. The yacht is accelerated to $u = 4.4$m/s in the first second. This leads to an encounter frequency of $0.53\frac{1}{\text{s}}$. The yacht is free in pitch and heave.

The solution-domain uses a wave-generation zone of 1λ and a wave-damping zone of 2λ. The free flow begins 1LoS in front of the yacht and ends 2LoS behind the yacht. The grid is generated using the OpenFOAM mesher snappyHexMesh, but with the use of some small in-house code and a lot of scripting to get a mesh of good quality with anisotropic refinement. The grid uses 100 cells per wave length and 20 cells per wave height. Depending on the part of the yacht, seven to nine prism-layers are applied leading to $y+$ values of 40 to 90 underwater. The kelvin-refinement ends in front of the wave-damping zone. The cells inside the kelvin-refinement have a size less or equal to 0.125m. The final mesh has 8.5E6 cells.

A modified $k - \omega$-SST turbulence model is used. The modification consist of a different production term as described in [1] and a correct consideration of the density-derivations for free-surface flows, compared to OpenFOAM's standard turbulence models. The timestep was

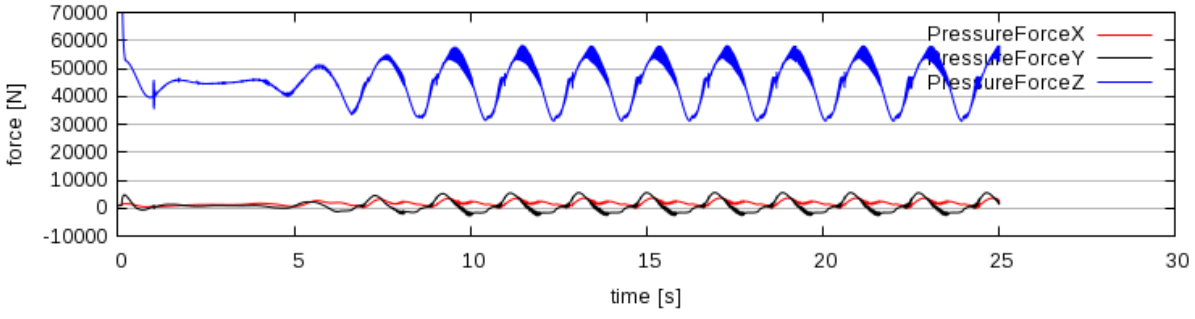

Figure 6: C40-design in head waves - pressure forces

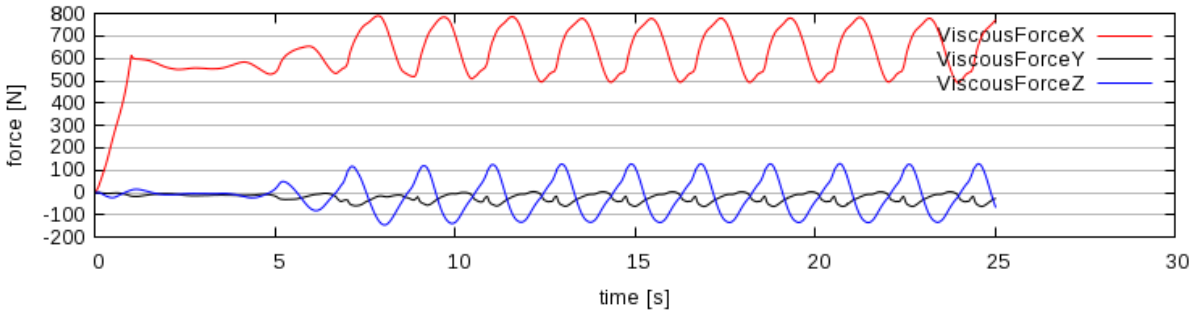

Figure 7: C40-design in head waves - viscous forces

set to 0.005s and the solver uses 5 SIMPLE-Loops. The simulation was calculated on a cluster with three knots, each with two 6-core CPUs. The simulation took about 65 hours.

Figures 6 and 7 show the pressure and the viscous forces. One can clearly see a periodic behavior and no significant disturbance due to wave reflections. The viscous force in x-direction has the most variation. This can be explained with ventilation under the hull composed of correct ventilation due to encountering a trough and incorrect numerical ventilation due to smearing of the free-surface. First simulations using a coarser grid (4.4E6 cells, three prism layers, coarser kelvin refinement) show much more variations in the viscous forces in the x-direction.

Figures 8 and 9 show a close view onto the hull and its wave system for two different times. Figure 8 shows the hull diving into the sea wave, whereas Figure 9 shows the hull with the bow knuckle significantly above the free-surface. In both cases, one can clearly see a smooth and good resolved kelvin wave pattern and furthermore breaking waves at the hull.

Figures 10 and 11 show wave patterns at different times. The end of the generation-zone and the beginning of the damping-zone are marked with two red y-planes in Figure 11. As one can see, the waves get damped in front of the outlet. The large scaled sea waves are not dampened completely at the outlet as expected for the chosen χ of 0.09. Apart from that, the small scaled wave-system of the yacht seems to be dampened completely at the outlet. The reason for this is first the length of the damping-zone, which is significantly longer than twice the wave length of the yacht induced waves. Therefore the damping for this small-scaled waves should be of a quality better than required. The second reason is the kelvin refinement ending in front of the damping-zone. At the y-max and y-min domain borders (the sides of the domain) the free traveling waves show no significant differences to each others. This underscores first the good wave propagation due to the 2nd order time discretization and second the suppression of wave reflections.

8 CONCLUSION

A new wave damping method was derived and investigated for monochromatic waves. The simulations show an overall good damping quality with reflections less than 2%. For different wave characteristics the same parameters leads to the best damping quality. Therefore the method can be seen as adjustment-free in the scope of the investigated waves. The damping quality for irregular or breaking waves has not been investigated and is an open topic for future investigations. Nevertheless, especially for irregular waves, which can be seen as a superposition

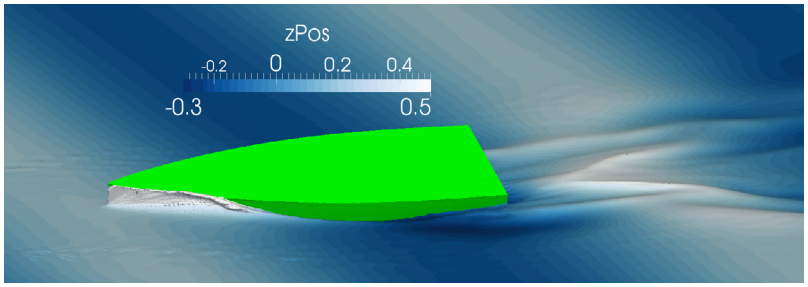

Figure 8: C40-design close-up at $t = 23.1$

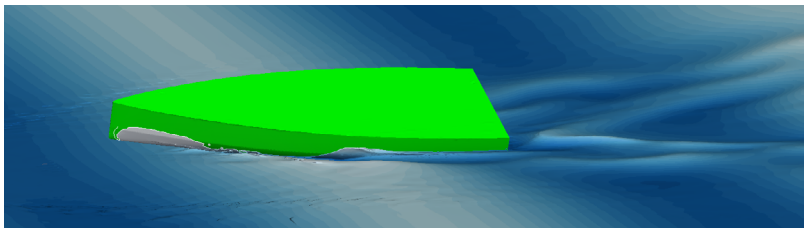

Figure 9: C40-design close-up at $t = 23.9$

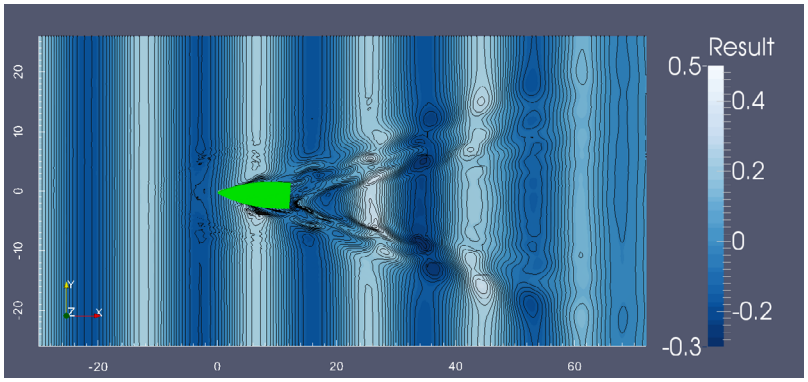

Figure 10: C40-design wave pattern at $t = 23.9$

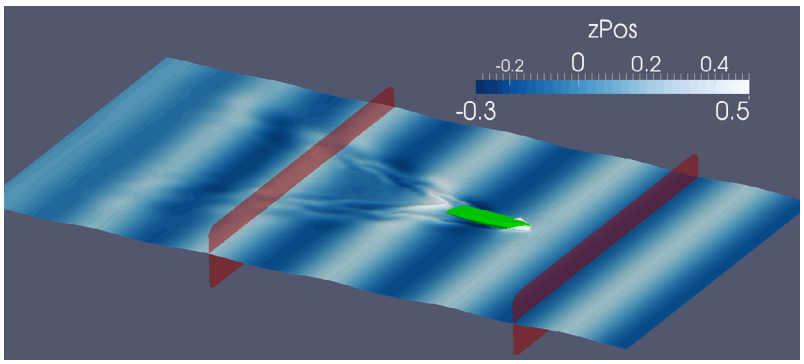

Figure 11: C40-design 3D view at $t = 23.1$

of regular waves, the authors expect a good damping quality, due to the adjustment-free behavior for monochromatic regular waves. The application of the method to a yacht in head waves emphasizes the user-friendly applicability, as it delivers a periodic solution with less variation just by activating the damping method with our optimized parameters.

REFERENCES

[1] Jacobsen, N.G., Fuhrman, D.R. and Fresdøe, J., A wave generation toolbox for the open-source CFD library: OpenFOAM®, *International Journal for Numerical Methods in Fluids*, (2012), **70**:1073–1088.

[2] Higuera, P., Lara, J.L. and Losada, I.J., Realistic wave generation and active wave absorption for Navier-Stokes models: Application to OpenFOAM®, *Coastal Engineering*, (2013), **71**:119–134.

[3] Hirt, C.W. and Nichols, B.D., Volume of Fluid (VOF) Method for the Dynamics of Free Boundaries, *Journal of Computational Physics*, (1981) **39**:201–225.

[4] Queutey, P. and Visonneau, M., An interface capturing method for free-surface hydrodynamic flows, *Computers & Fluids*, (2007), **36**:1481–1510.

[5] Wackers, J., Koren, B., Raven, H.C., van der Ploeg, A., Starke, A.R., Deng, G.B., Queutey, P., Visonneau, M., Hino, T. and Ohashi, K., Free-surface viscous flow solution methods for ship hydrodynamics, *Archives of Computational Methods in Engineering*, (2010), **18**:1–41.

[6] Soeding, H., How to integrate free motion of solids in fluids, *4th Numerical Towing Tank Symposium*, Hamburg-Germany, (2001).

[7] Meyer, J., Renzsch, H., Graf, K. and Slawig, T., Advanced CFD-Simulations of free-surface flows around modern sailing yachts using a newly developed OpenFOAM solver, *The 22nd Chesapeake Sailing Yacht Symposium*, Annapolis-Maryland, (2016).

[8] Choi, J and Yoon, S.B., Numerical simulations using momentum source wave-maker applied to RANS equation model, *Coastal Engineering*, (2009), **56**:1043–1060.

[9] Park, J.C., Kim, M.H. and Miyata, H., Fully non-linear free-surface simulations by a 3D viscous numerical wave tank, *International Journal for Numerical Methods in Fluids*, (1999), **29**:685–703.

[10] Perić, R. and Abdel-Maksoud, M., Reliable Damping of Free Surface Waves in Numerical Simulations, *Ship Technology Research*, (2016), **63**.

[11] Perić, R., Internal generation of free surface waves and application to bodies in cross sea, MSc Thesis, *Schriftenreihe Schiffbau*, Hamburg University of Technology, Hamburg-Germany, (2013).

[12] Ursell, F., Dean, R.G. and Yu, Y.S., Forced small-amplitude water waves: a comparison of theory and experiment, *Journal of Fluid Mechanics*, (1960), **7**:33–52.